Volume 10 | Number 27 | 21 July 2018 | Pages 12857–13292

Nanoscale

rsc.li/nanoscale

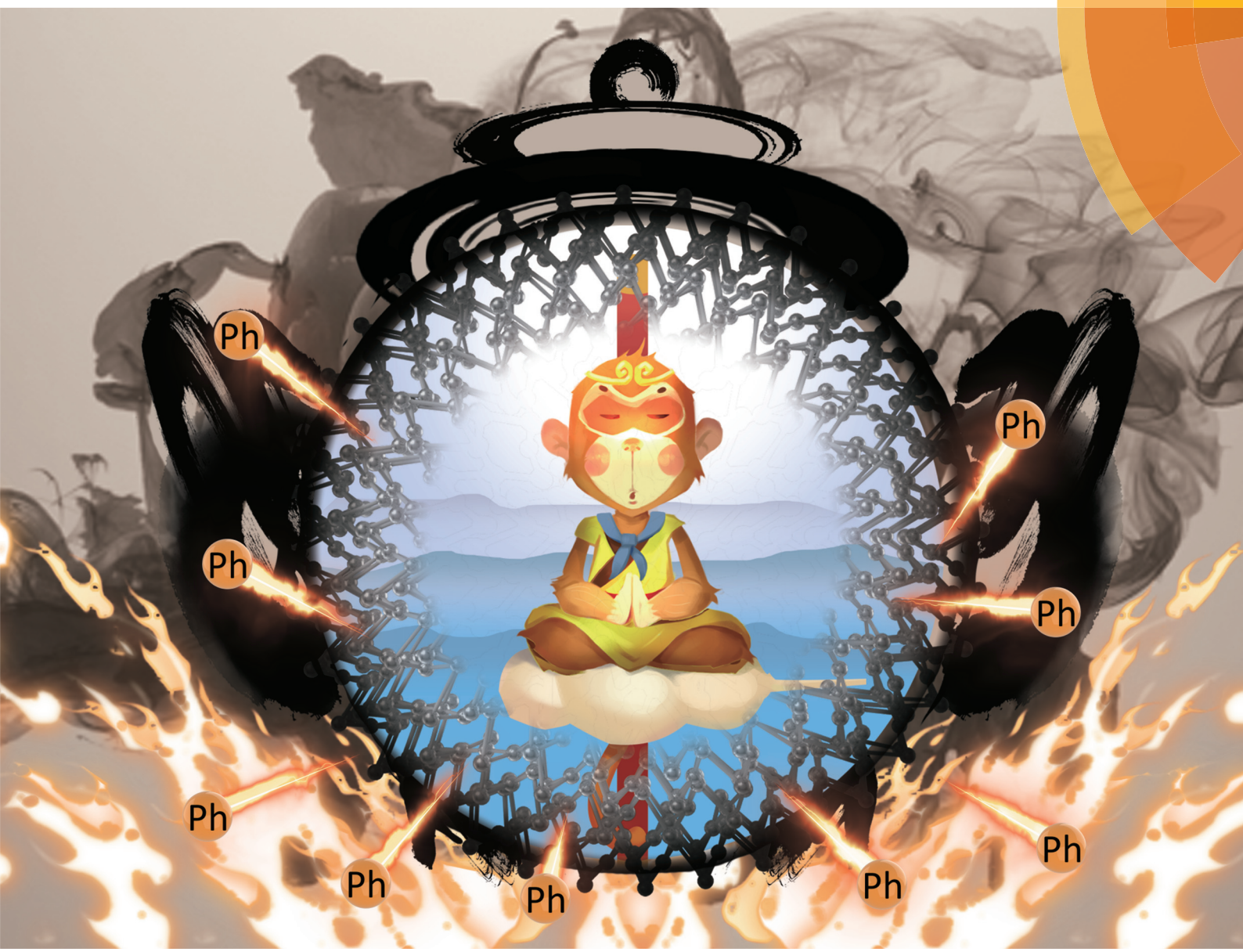

ISSN 2040-3372

ROYAL SOCIETY OF CHEMISTRY

PAPER
Zhibin Gao, Fang Tao and Jie Ren
Unusually low thermal conductivity of atomically thin 2D tellurium

NCNST

Nanoscale

PAPER

View Article Online
View Journal | View Issue

Cite this: *Nanoscale*, 2018, **10**, 12997

Unusually low thermal conductivity of atomically thin 2D tellurium†

Zhibin Gao, Fang Tao and Jie Ren *

Received 27th February 2018,
Accepted 25th April 2018

DOI: 10.1039/c8nr01649f

rsc.li/nanoscale

Tellurium is a high-performance thermoelectric material due to its superior electronic transport and low lattice thermal conductivity (κ_L). Here, we report the ultralow κ_L in the monolayer tellurium, *i.e.*, tellurene, which has been successfully synthesized in recent experiments. We find that tellurene has a compellingly low room temperature κ_L of 2.16 and 4.08 W m^{-1} K^{-1} along the armchair and zigzag directions, respectively, which is lower than any reported values for other 2D materials. We attribute this unusually low κ_L to the soft acoustic modes, the extremely low-energy optical modes and the strong scattering among optical–acoustic phonons, which place tellurene as a potential novel thermoelectric material. Finally, we show that κ_L is proportional to the largest acoustic phonon frequency (ω_D^a) and the lowest optical phonon frequency at the Γ point (ω_Γ^o) in 2D materials, which reflect both harmonic and anharmonic thermal properties, respectively.

1. Introduction

Graphene, probably the most studied 2D system in the history of science, displays record thermal conductivity,[2] comparable to single-wall carbon nanotubes.[3] Also other 2D materials such as hexagonal BN display much higher thermal conductivities than most 3D bulk materials. Here we show that an atomically thin monolayer of Te, which has been synthesized recently, has an unusually low lattice thermal conductivity. Minimizing thermal conductivity is very important for thermoelectrics to efficiently convert unavoidable waste heat to electricity, since the figure of merit zT is inversely proportional to this quantity.

Specifically, the figure of merit of a thermoelectric material is expressed as $zT = S^2\sigma T/(\kappa_e + \kappa_L)$, where S, σ, T, κ_e and κ_L are the Seebeck coefficient, electric conductivity, absolute temperature, electronic thermal conductivity and lattice thermal conductivity, respectively. Hunting for optimum zT materials needs not only a maximum power factor ($S^2\sigma$) but also simultaneously a minimum thermal conductivity ($\kappa_e + \kappa_L$). Since the electric properties S, σ and κ_e couple strongly with each other and are interdependent in complicated ways, optimization of zT becomes an arduous issue to realize the waste heat recovery.[4] Fortunately, owing to the different and separate scale of the mean free paths of electrons and phonons, κ_L is a relatively independent parameter in zT. Therefore, seeking materials of ultralow κ_L becomes an effective way to achieve high thermoelectric performance,[5] and over the past few decades, considerable progress has been made in decreasing κ_L, to realize the so-called "phonon-glass electron-crystal behavior".

As an accepted rule of thumb,[6,7] we sum up some of the conditions in dielectric materials that can lead to ultralow κ_L: (i) complex crystal structure (such as skutterudites,[8] clathrates,[9,10] and embedded nanoparticles[11]), (ii) a large average atomic mass, (iii) weak interatomic bonding, and (iv) strong anharmonicity (such as SnSe[12]). A small Debye temperature, θ_D, always originates from a combination of heavy elements (ii) and low atomic coordination (iii).[13] Furthermore, ultralow κ_L can also be obtained through high disorder,[14] resonant bonding (such as rocksalt group IV–VI compounds[15] and in-filled $CoSb_3$[16]) and lone electron pairs (such as group I–V–VI_2 compounds[17] and InTe[18]).

On the one hand, bulk Te has recently been shown to be a superior thermoelectric material with zT = 1.0[1] in addition to being a topological insulator,[19,20] since its room temperature κ_L was experimentally found to be as low as 1.96–3.37 W m^{-1} K^{-1}.[21] In 2017, Qin *et al.*[22] grew a controllable and large-size 2D selenium, belonging to the same Group VI family as tellurene. Recently, Zhu *et al.*[23] and Chen *et al.*[24] have successfully synthesized ultrathin layers of tetragonal β-tellurene on highly oriented pyrolytic graphite (HOPG) using molecular beam epitaxy, which has much larger carrier mobility than MoS_2 and is highlighted in an exclusive report for its potential implications.[25] Xie *et al.*[26] obtain 2D Te nanosheets *via* liquid-phase exfoliation. Moreover, Liu *et al.*[27] and Qiao *et al.*[28] also indicate that few layer tellurene has extraordinary electronic transport properties and can be made high-performance field-effect transistors by Wang *et al.*[29] Yet, κ_L of this intrinsic 2D

Center for Phononics and Thermal Energy Science, China-EU Joint Center for Nanophononics, Shanghai Key Laboratory of Special Artificial Microstructure Materials and Technology, School of Physics Sciences and Engineering, Tongji University, Shanghai 200092, China. E-mail: Xonics@tongji.edu.cn

†Electronic supplementary information (ESI) available. See DOI: 10.1039/C8NR01649F

tellurene structure is far from clear. In this letter, we explore the intrinsic κ_L of monolayer β-tellurene.

On the other hand, Dresselhaus *et al.* have pointed out that low dimensional materials (such as 2D materials) can further enhance the electronic performance compared to their 3D counterparts due to quantum confinement.[30] However, 2D materials usually also have larger κ_L than their 3D bulk counterparts due to the significant contributions of the out-of plane (ZA) modes.[31,32] This counteracts the huge potential of a 2D material with better thermoelectric zT. As such, seeking 2D materials of ultralow κ_L is significant to fabricate superior and miniaturized thermoelectric devices.[33] Therefore, although 2D tellurene is supposed to have good electronic properties, its thermal properties are crucial and will strongly impact tellurene's potential to possess good thermoelectric performance.

In this letter, we found that tellurene has unusually low room temperature κ_L of merely 2.16 and 4.08 W m^{-1} K^{-1} along the armchair and zigzag directions, respectively. Those values, although obtained from the 2D crystalline tellurene, are comparable to the bulk Te, which is quite counterintuitive given the well-known trend that 2D materials have usually larger κ_L than their 3D counterpart due to the significant ZA mode contribution to the κ_L.[31,32] Moreover, we find that tellurene has the lowest recorded κ_L among the 2D material family to date. Therefore, we carefully scrutinize the underlying mechanism of ultralow κ_L of tellurene from the aspects of harmonic and anharmonic properties in the following.

2. Lattice thermal conductivity

In semiconductors and insulators, heat is mainly carried by phonons. The anisotropic in-plane lattice thermal conductivity under the relaxation time approximation can be calculated as the sum of the contributions of all phonon modes λ with the wave vector **q**:

$$\kappa_{\alpha\beta} = \frac{1}{V}\sum_{\lambda} C_{\lambda} v_{\lambda\alpha} v_{\lambda\beta} \tau_{\lambda}, \quad (1)$$

where V is the crystal volume, and λ denotes a phonon mode with different wave vectors and branch indexes. α and β denote the Cartesian directions. C_{λ} is the specific heat per mode, $v_{\lambda\alpha}$ and τ_{λ} are the velocity components along the α direction and the relaxation time of the phonon mode λ. κ_L can be obtained by solving the phonon Boltzmann transport equation that is related to the harmonic and anharmonic interatomic force constants.

κ_L is an intensive property. Hence, a value of thickness needs to be chosen in 2D materials when compared with the 3D counterpart. In order to make it more clear and consistent, we also use the thermal sheet conductance ("2D thermal conductivity") with the unit W K^{-1} as it is the most unequivocal variable in 2D materials. The thickness of tellurene (6.16 Å) is taken as the summation of the buckling distance and the van der Waals (vdW) radii of a Te atom,[36,37] which is in good agreement with our calculated value obtained by artificially stacking tellurene layers.

The crystal structure information of tellurene is shown in section I of the ESI.† Fig. 1 shows the calculated κ_L of tellurene along the armchair (x-axis) and zigzag (y-axis) directions as a function of temperature, as well as the collected κ_L data of bulk Te for comparison. The intrinsic κ_L (only consider the phonon–phonon scattering) at room temperature of tellurene along the x and y directions are 2.16 and 4.08 W m^{-1} K^{-1}, respectively. As mentioned above, due to the symmetry the κ_L of bulk Te is isotropic parallel to the helical chains but anisotropic when perpendicular to the chains.[34,38] We compare the κ_L between tellurene and bulk Te parallel to the helical chains. These values of tellurene (red solid triangle) are comparable to and even smaller than the theoretical result[34] of bulk Te along the helical chains direction (open purple triangle) in all of the temperature range, which is in contrast to what happens in other layered 2D materials (such as graphene compared to graphite). Furthermore, κ_L along the x direction is only one half of that in the y direction, indicating a large anisotropic thermal transport in tellurene.

The minimum lattice thermal conductivity κ_{min} of bulk Te according to the Cahill model[1,35] is shown as a reference. Additionally, in real experiment and practical devices, boundary scattering will further reduce the κ_L of a material with finite size (Fig. S1 in the ESI†). Ultralow κ_L in tellurene comparable with bulk Te deviates from the well-known trend that 2D materials have usually larger κ_L than their 3D counterpart,[31,32] encouraging us to explore the physical reason behind it.

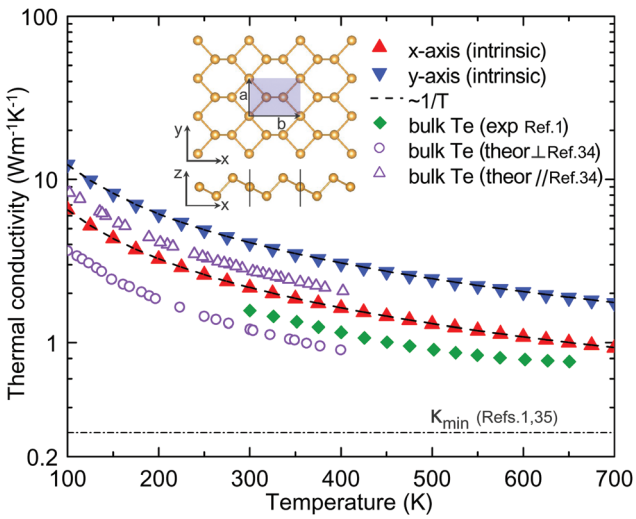

Fig. 1 Lattice thermal conductivity of tellurene as a function of temperature. A ball and stick model of tellurene in top and side views is shown in the inset. The primitive cell is indicated by the blue shading in the top view. a and b are the lattice vectors spanning the 2D lattice. Black dashed lines are $1/T$ fitting of temperature dependent κ_L. The experimental data[1] of bulk Te are collected in green rhombic dots. The theoretical results[34] are gathered in purple triangles/circles lying parallel/perpendicular to the bulk helical chains. The dashed lines are provided as a guide to the eye. Red and blue solid triangles are the intrinsic κ_L we obtained from the phonon Boltzmann transport equation considering phonon–phonon scattering. The dash dotted line is the lower limit κ_{min} of bulk Te from the previous experiment[1] that is based on the Cahill model.[35]

The thermal sheet conductances of tellurene along the x and y directions are 1.33 and 2.51 nW K^{-1}, which are also the lowest values in the 2D crystalline family to date (Table S2 in the ESI†). Furthermore, we found that κ_L of tellurene matches well with T^{-1} behavior, indicating a dominant Umklapp process of phonon scattering that causes thermal resistivity. This nice T^{-1} curve is common in other heavy elements[39] and recently was also experimentally observed in bulk Te.[1] The fitting information is shown in section II of the ESI.† The unusually low and anisotropic κ_L of tellurene will be explained physically from both the harmonic and anharmonic properties in the following sections.

3. Soft harmonic properties

Tellurene has three atoms in each unit cell shown in the inset of Fig. 1, so it possesses three acoustic and six optical phonon modes. For 2D materials, in the long wavelength limit, very close to the Γ point, the LA and TA modes are linear in $\mathbf{q}$, whereas the ZA mode is quadratic,[40] with the coefficients given by 2D continuum elasticity theory.[41] But when $\mathbf{q}$ is slightly far away from Γ, ZA mode will have a near-linear trend. The details of this 2D continuum elasticity theory[41] in tellurene are discussed in section III of the ESI.†

The corrected phonon dispersion and phonon density of states (PDOS) of tellurene are shown in Fig. 2a and b (also in Fig. S2 in section III of the ESI†). LA and TA phonon modes along Γ-X are much lower than those in the Γ-Y direction, implying a smaller θ_D in the x direction. The calculated flexural rigidities $D(\Gamma\text{-}X)$ and $D(\Gamma\text{-}Y)$ are 0.37 and 0.40 eV in tellurene along the x and y directions shown in Fig. S2 of the ESI,† which describes the flexural response to the out-of-plane stress of materials. These values of tellurene are about a quarter of graphene (1.4 eV (ref. 41)) and phosphorene (1.55 eV (ref. 41)), indicating that tellurene is much softer than graphene and phosphorene. Another alternative method is to correct force constants by rigorously applying the translation and rotation symmetries.[40]

Moreover, an asymmetric optical phonon branch in the magenta line shown in Fig. 2a, like a waterfall, suddenly falls into the very low frequency region. We found the corresponding optical mode vibrates along the y direction as shown in the inset of Fig. 3a, so that we call it TO$_y$ in the following. Group velocities, defined as $\upsilon = \partial\omega/\partial q$, are shown in Table S1 of the ESI.† These ultra-small sound velocities will contribute to the fact that tellurene has unusually low κ_L because κ_L is proportional to υ^2 based on eqn (1).

From tellurene's phonon spectrum, the ZA mode along both directions is much flat (smaller D),[41] possessing much lower υ. As we all know, the ZA mode plays a crucial role in the κ_L of 2D materials.[31,32] For instance, 75% κ_L derived from the ZA mode in graphene.[42] Thus, abundance of such soft ZA modes with much lower υ significantly weakens their role in the thermal conductivity of tellurene, which is another reason for ultralow κ_L. We also calculated the frequency-resolved κ_L for tellurene. Similar to graphene and other 2D materials, in

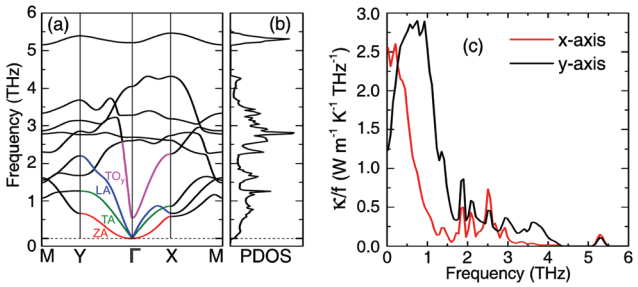

Fig. 2 (a) Phonon band structures and (b) phonon density of states (PDOS) of tellurene. Three acoustic phonon branches, which originate from the Γ-point of the Brillouin zone, correspond to an out-of-plane (ZA) mode, an in-plane transverse (TA) mode, and an in-plane longitudinal (LA) mode. The asymmetric waterfall-like transverse optical phonon mode along y axis (TO$_y$) is also marked. The dashed lines are provided as a guide to the eye. (c) Frequency-resolved thermal conductivity for tellurene in the x and y directions at room temperature.

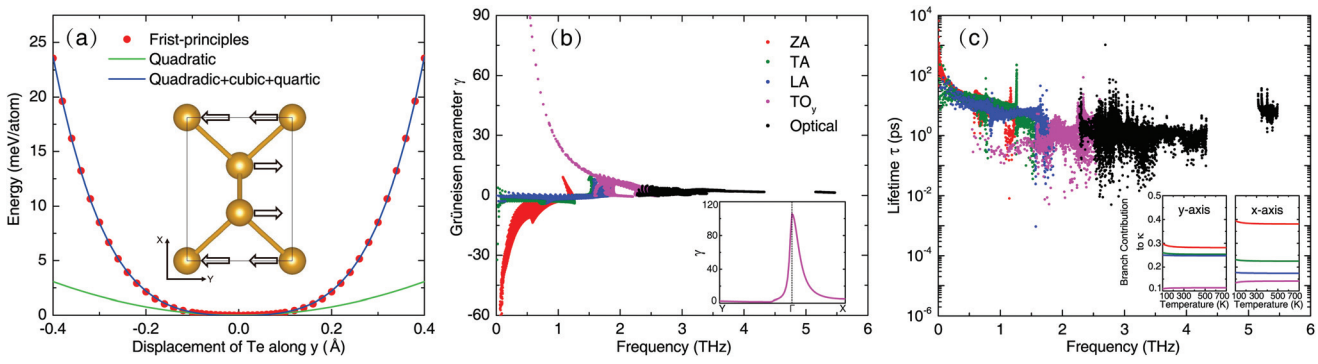

Fig. 3 (a) Anharmonic frozen-phonon potential with quadratic and polynomial fitting. The inset shows the vibration direction of the lowest-energy TO$_y$ phonon mode. (b) The Grüneisen parameter γ as a function of the phonon frequency. The inset shows the γ of the waterfall-like optical phonon mode (TO$_y$) along both directions. (c) Dependence of the phonon relaxation time on frequency at room temperature. The inset shows the normalized contribution of all acoustic and TO$_y$ phonon modes to κ_L as a function of temperature along both directions.

tellurene low frequency phonons dominate the contribution of κ_L in both the x and y directions shown in Fig. 2c. As will be discussed later, waterfall-like TO_y mode enhances the scattering between acoustic and optical phonon modes in tellurene. Therefore, the contribution of the acoustic phonon modes to the total κ_L will be weakened.

The mechanical properties of tellurene calculated based on elastic solid theory[36] are shown in Table S1 of ESI.† Young's modulus and Poisson's ratio of tellurene in the y direction are about two times larger than those in the x direction. Tellurene has very small E and Poisson's ratio ν along both directions, indicating a lower vibrational strength.[43] As we have discussed above, a small θ_D means average low phonon frequency. A small θ_D, combined with low υ, always implies a weak interatomic bonding, which will decrease the κ_L of heavy tellurene (criteria ii and iii). This is another effect from harmonic properties that explains why tellurene has an unusually low and anisotropic κ_L.

4. Giant Grüneisen parameter

Strong anharmonicity in materials can lead to low κ_L (criterion iv). The Grüneisen parameter, γ, measures the effect of volume change of a crystal on the thermal expanded phonon vibrations so that large γ indicates a large bonding anharmonicity in materials. This giant anharmonicity of the TO_y phonon mode is strongly related to the chemical bonding and distortion potential[12] shown in Fig. 3a. We move all atoms along its eigenvector and the symmetric potential intensely deviates from the quadratic function. The strong anharmonicity of the TO_y phonon mode can be further confirmed by a polynomial fitting, which is consistent with the giant γ in the inset of Fig. 3b. The large γ of the TO_y phonon branch enhances the scattering rates and anharmonicity, leading to the ultralow κ_L of tellurene.

To further explore the γ distribution, we calculated γ for the whole frequency spectrum in Fig. 3b. Below the frequencies of 0.5 THz (see also Fig. 2a), there is no obvious acoustic–optical (a–o) phonon scattering and the ZA mode has the largest γ. As a matter of fact, κ_L is both proportional to the anharmonic interaction (matrix) elements and the inverse of phase space volume P_3. The former is closely related to the frequency-dependent γ and the latter describes all available three-phonon scattering processes that need to satisfy the energy and momentum conservation simultaneously.[15,44,45] The calculated P_3, shown in Fig. S3 in section VI of the ESI,† indicates that three-phonon scattering channels in tellurene do not vary too much. Hence, ultralow κ_L mainly stems from the large γ, rather than the increase of scattering channels.

In the frequency range of 0.5–2.0 THz, γ of ZA, TA, LA and TO_y phonon modes suddenly jump, indicating a giant anharmonic scattering change of interaction (matrix) elements between the acoustic and optical phonons. This phenomenon can also be mapped in the phonon dispersion shown in Fig. 2a. The giant γ induced by the large a–o phonon scattering is also the origin of the ultralow κ_L of SnSe,[12] single-layer transition metal dichalcogenides,[46] phosphorus,[47] and rocksalt structures,[15] but when absent, γ leads to the ultrahigh κ_L of boron arsenide.[7]

In the inset of Fig. 3b, we plot the corresponding γ for the TO_y phonon mode along the x and y directions. One can clearly see an asymmetric giant γ along both directions and the γ in the x direction is relatively larger than that in the y direction, indicating a stronger optical–acoustic phonon scattering so that tellurene has a lower κ_L in the x direction in the frequency range of 0.5–2.0 THz [see Fig. 2(c)]. Therefore, in the x direction the stronger anharmonic scattering together with the weaker harmonic properties both lead to the unusually low κ_L in the x direction, resulting in an anisotropic κ_L in tellurene.

5. Strong optical–acoustic phonon scattering

A finite κ_L is an outcome of the phonon–phonon scattering.[48,49] As is evident in Fig. 3c, in the range of 0.5–2.0 THz, the calculated phonon lifetimes of ZA, TA, LA and TO_y phonon modes are significantly shortened due to the strong a–o scattering. A smaller phonon lifetime will result in a smaller κ_L according to eqn (1), and the contribution of these four phonon branches is shown in the inset of Fig. 3c. When putting graphene on the substrate, the room temperature κ_L will significantly decrease from 3000–5000 W m^{-1} K^{-1} of suspended graphene[2] to 600 W m^{-1} K^{-1} of supported graphene,[31,32] due to the large suppression of the ZA mode contribution by substrates,[31] since 75% of graphene's κ_L are carried by the ZA phonon mode.[42] Due to the strong a–o scattering in tellurene, the ZA mode contribution has been reduced to 38.2% and 28.3% along the x and y directions. For tellurene, the ZA mode contribution is largely suppressed by the soft dispersion, along with the large scattering from the TO_y phonon mode, finally resulting in the ultralow κ_L. When considering tellurene of finite size, the boundary scattering will further decrease the κ_L. The corresponding length-dependent κ_L for suspended tellurene is shown in Fig. S4 in section V of the ESI.†

Moreover, Fig. 4 shows that tellurene has the lowest κ_L based on our collected data (Table S2 in the ESI†) of 2D materials. We found that the largest acoustic phonon frequency ω_D^a projected in green dots and the lowest optical phonon frequency at Γ point ω_Γ^o projected in blue dots are two good descriptors to estimate κ_L. Heat is mainly carried by low frequency acoustic phonons in dielectric materials.[50] On the one hand, a lower ω_D^a means a weaker acoustic phonon vibration,[5] indicating a poor performance in thermal transport and a lower κ_L from the harmonic viewpoint. On the other hand, ω_Γ^o decides the energy gap between the acoustic (a) and optical (o) phonons. There are four kinds of processes in the three-phonon scattering according to the energy and momentum conservation conditions: (a, a, a), (a, a, o), (a, o, o) and (o, o, o) in which the dominant scattering channels that contrib-

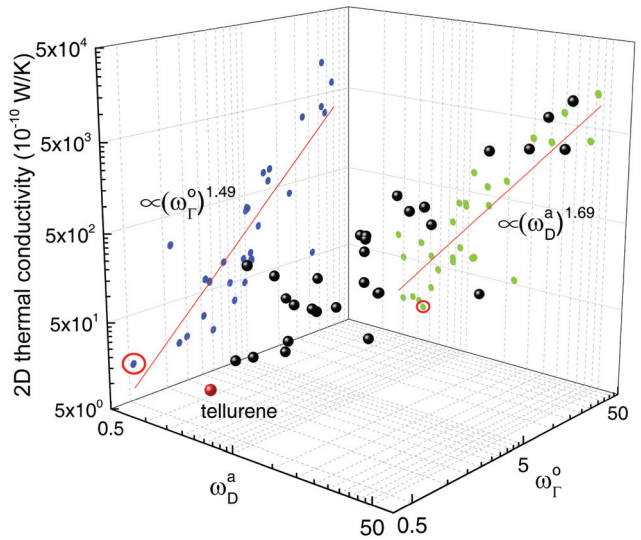

Fig. 4 Room temperature 2D κ_L in W K^{-1} as a function of ω_D^a and ω_Γ^o, which are the largest acoustic phonon frequency and the lowest optical phonon frequency at the Γ point in THz. The projected data are fitted as $\kappa_L \propto (\omega_D^a)^{1.69}$ and $\kappa_L \propto (\omega_\Gamma^o)^{1.49}$. κ_L in the 3D coordinate axis are indicated by black points. The projections on the κ_L–ω_Γ^o plane and κ_L–ω_D^a plane are denoted by blue and green dots. Tellurene is marked as a red point with the lowest κ_L and two red circles are the separate projections. Details of these data are collected in Table S2 in the ESI.†

ute most to the three-phonon phase space in the majority of materials are the (a, a, o) group, resulting in the main thermal resistance in materials.[7,44] Therefore, ω_Γ^o is the key factor in three-phonon scattering processes, which is closely related to the anharmonicity.

Hence, ω_D^a and ω_Γ^o are two good characteristics of κ_L from both harmonic and anharmonic aspects. After projection, we find that 2D κ_L can be fitted as $\kappa_L \propto (\omega_D^a)^{1.69}$ and $\kappa_L \propto (\omega_\Gamma^o)^{1.49}$. Note that two exponents in the above trends exhibit some uncertainty based on the limitedly published values of κ_L, thus 1.69 and 1.49 are not very rigorous but the trends between κ_L and ω_D^a and ω_Γ^o are universal (at least, positive correlations).

For 3D bulk materials, there are many formulas such as Debye,[51] Slack,[6] Klemens,[52] Dugdale and McDonald,[53] Debye–Callaway[54] and so on. However, so far no one gives a counterpart formula for 2D nonmetallic crystal materials. For the bulk materials at temperatures above θ_D, Umklapp phonon–phonon scattering is often the dominant scattering effect, which situation also appears in 2D materials. The widely accepted Slack model[6] for 3D materials is proposed under the same assumption. We are wondering whether this model could also be used for 2D materials. For comparison, we list the Slack model[6,55] as follows:

$$\kappa_L \propto \frac{a^4 \rho (\omega_D^a)^3}{\gamma^2 T}, \quad (2)$$

where a^3, ρ and γ are the average volume occupied by one atom of the crystal, density and the acoustic phonon Grüneisen parameter. However, based on our collected data in Fig. 4, κ_L of 2D materials is proportional to $(\omega_D^a)^{1.69}$, which evidently violates the above Slack formula. Therefore, our results indicate that the Slack model originally proposed for 3D materials is not generally applicable to 2D materials.

In order to unveil the source of this violation, we analyse the difference in phonon spectra and some related physical quantities between 2D and 3D materials. The fundamental difference stems from the acoustic phonon modes. In 3D materials, there are three linear acoustic phonon modes, whereas in 2D, there are only two linear modes and one quadratic ZA acoustic phonon mode whose vibration direction is in the out-of-plane. As we discussed before, for 2D materials, in the long wavelength limit, very close to the Γ point, the LA and TA modes are linear in **q**, whereas the ZA mode is quadratic. Hence, group velocities of ZA phonon modes close to Γ are proportional to **q**, different from the constant group velocities in 3D materials. Furthermore, density of states (DOS) is another difference between 2D and 3D materials. The DOS of three linear acoustic phonon modes in 3D materials are proportional to $(\omega_D^a)^2$. After integration, the power law is in line with the Slack model. But an exclusive parabolic ZA mode would lead to a constant DOS, indicating a different κ_L behavior of 2D compared with 3D materials. More details are shown in section VI of the ESI.†

Based on eqn (1), the unique ZA mode behaviors of group velocities and DOS contribute to the non-cubic power law relationship between ω_D^a and κ_L. Nevertheless, these two trends reveal that ω_D^a and ω_Γ^o are two relevant descriptors for κ_L. ω_D^a reflects the strength of acoustic phonon vibrations and group velocities. ω_Γ^o discloses the important gap between acoustic and optical modes that is very crucial for the optical–acoustic phonon scattering rates and scattering channels.[7,15,45] A lower ω_Γ^o will enhance the three-phonon scattering processes and will have a significant impact on the anharmonicity and attenuation on κ_L.

6. Conclusion

In conclusion, we have theoretically explored the unusually low thermal properties of tellurene by the first-principles calculations and phonon Boltzmann transport. To trace the ultralow κ_L, we unveil the reasons from both the harmonic and anharmonic aspects. Tellurene consists of heavy atomic mass (criterion ii). From the harmonic view of phonon dispersion and elasticity, low Debye temperature, group velocities of acoustic phonons, Young's modulus, and shear modulus reveal the weak phonon vibrations and interatomic bonding that lead to the unusually low κ_L in tellurene (criteria iii). For anharmonicity, large γ, strong acoustic-optical phonon scattering and large phonon–phonon anharmonic scattering rates are shown to illustrate the strong anharmonicity in tellurene (criterion iv). These convincing pieces of evidence have verified the unusually low κ_L in atomically thin 2D tellurium. Finally, we found that κ_L is proportional to the largest acoustic phonon frequency (ω_D^a) and the lowest optical phonon frequency at the Γ

point (ω_T^0) for reported 2D materials. These two frequencies reflect the thermal properties from both harmonic and anharmonic aspects.

Coupled with the superior electronic transport,[1,23,27–29] we hope that ultralow κ_L tellurene would shed light on the implication for the thermoelectric field in the future. Thickness-dependent κ_L is also an interesting open question to understand the thermal transport property in few-layer tellurene.

7. Methods

Our quantitative predictions were obtained by performing density functional theory (DFT) and by solving the phonon Boltzmann transport equation (BTE). We performed density functional theory calculations as implemented in the Vienna Ab initio simulation package (VASP)[56,57] with a plane-wave cutoff of 300 eV, 70% higher than the maximum recommended cutoff for the pseudopotentials. The Perdew–Burke–Ernzerhof (PBE) exchange–correlation functional[58] along with the projector-augmented wave (PAW) potentials[59,60] were used. The energy convergence value in a self-consistent field (scf) loop is selected as 10^{-8} eV and the maximum Hellmann–Feynman force is less than 0.001 meV Å^{-1}. Phonon frequencies and group velocities are calculated by the diagonalization of the dynamical matrix. Compared with single-mode relaxation time approximation (SMRTA), iterative BTE schemes are adopted, which overcome the weakness of underestimating the lattice thermal conductivity.[7,61] Harmonic interatomic force constants (IFCs) are obtained using Phonopy[62] with a $10 \times 10 \times 1$ supercell, while ShengBTE[45,63,64] is utilized to extract the anharmonic IFCs by solving the linearized phonon Boltzmann transport equation. A converged cutoff of 0.55 nm for the interaction range and a q-grid of $100 \times 100 \times 1$ were employed after testing. A $4 \times 4 \times 1$ supercell with a $3 \times 3 \times 1$ Monkhorst–Pack k-point mesh is used for IFC calculations.

Conflicts of interest

There are no conflicts to declare.

Acknowledgements

Z. G. is grateful for the hospitality of Prof. David Tománek, Michigan State University, where this work was initiated, and the China Scholarship Council (CSC) for financial support (to C. S., 201706260027). We thank David Tománek, Jesús Carrete and Dan Liu for very helpful discussions and their critical reading of the manuscript, as well as for correcting the ZA mode dispersion. Z. G., F. T. and J. R. were supported by the National Natural Science Foundation of China with grant no. 11775159, the National Natural Science Foundation of Shanghai with grant no. 18ZR1442800, the National Youth 1000 Talents Program in China, and the startup grant at Tongji University, and the Opening Project of Shanghai Key Laboratory of Special Artificial Microstructure Materials and Technology. Computational resources have been provided by the Tongji University and Michigan State University High Performance Computing Center.

References

1 S. Lin, W. Li, Z. Chen, J. Shen, B. Ge and Y. Pei, *Nat. Commun.*, 2016, **7**, 10287.
2 A. A. Balandin, S. Ghosh, W. Bao, I. Calizo, D. Teweldebrhan, F. Miao and C. N. Lau, *Nano Lett.*, 2008, **8**, 902–907.
3 S. Berber, Y.-K. Kwon and D. Tománek, *Phys. Rev. Lett.*, 2000, **84**, 4613–4616.
4 G. J. Snyder and E. S. Toberer, *Nat. Mater.*, 2008, **7**, 105–114.
5 L.-D. Zhao, S.-H. Lo, Y. Zhang, H. Sun, G. Tan, C. Uher, C. Wolverton, V. P. Dravid and M. G. Kanatzidis, *Nature*, 2014, **508**, 373–390.
6 G. A. Slack, *J. Phys. Chem. Solids*, 1973, **34**, 321–335.
7 L. Lindsay, D. Broido and T. Reinecke, *Phys. Rev. Lett.*, 2013, **111**, 025901.
8 R. Wei, G. Huiyuan, Z. Zihao and Z. Lixia, *Phys. Rev. Lett.*, 2017, **118**, 245901.
9 W. G. Zeier, J. Schmitt, G. Hautier, U. Aydemir, Z. M. Gibbs, C. Felser and G. J. Snyder, *Nat. Rev. Mater.*, 2016, **1**, 16032.
10 T. Tadano, Y. Gohda and S. Tsuneyuki, *Phys. Rev. Lett.*, 2015, **114**, 095501.
11 W. Zhao, Z. Liu, Z. Sun, Q. Zhang, P. Wei, X. Mu, H. Zhou, C. Li, S. Ma, D. He, P. Ji, W. Zhu, X. Nie, X. Su, X. Tang, B. Shen, X. Dong, J. Yang, Y. Liu and J. Shi, *Nature*, 2017, **549**, 247–251.
12 C. W. Li, J. Hong, A. F. May, D. Bansal, S. Chi, T. Hong, G. Ehlers and O. A. Delaire, *Nat. Phys.*, 2015, **11**, 1063.
13 J. Carrete, N. Mingo and S. Curtarolo, *Appl. Phys. Lett.*, 2014, **105**, 101907.
14 H. Liu, X. Shi, F. Xu, L. Zhang, W. Zhang, L. Chen, Q. Li, C. Uher, T. Day and G. J. Snyder, *Nat. Mater.*, 2012, **11**, 422–425.
15 S. Lee, K. Esfarjani, T. Luo, J. Zhou, Z. Tian and G. Chen, *Nat. Commun.*, 2014, **5**, 3525.
16 W. Zhao, P. Wei, Q. Zhang, H. Peng, W. Zhu, D. Tang, J. Yu, H. Zhou, Z. Liu, X. Mu, D. He, J. Li, C. Wang, X. Tang and J. Yang, *Nat. Commun.*, 2015, **6**, 6197.
17 M. D. Nielsen, V. Ozolins and J. P. Heremans, *Energy Environ. Sci.*, 2013, **6**, 570–578.
18 M. K. Jana, K. Pal, U. V. Waghmare and K. Biswas, *Angew. Chem., Int. Ed.*, 2016, **55**, 7792–7796.
19 L. A. Agapito, N. Kioussis, W. A. Goddard III and N. Ong, *Phys. Rev. Lett.*, 2013, **110**, 176401.
20 M. Hirayama, R. Okugawa, S. Ishibashi, S. Murakami and T. Miyake, *Phys. Rev. Lett.*, 2015, **114**, 206401.
21 C. Y. Ho, R. W. Powell and P. E. Liley, *J. Phys. Chem. Ref. Data*, 1972, **1**, 279–421.

22 J. Qin, G. Qiu, J. Jian, H. Zhou, L. Yang, A. Charnas, D. Y. Zemlyanov, C.-Y. Xu, X. Xu, W. Wu, H. Wang and P. D. Ye, *ACS Nano*, 2017, **11**, 10222–10229.
23 Z. Zhu, X. Cai, S. Yi, J. Chen, Y. Dai, C. Niu, Z. Guo, M. Xie, F. Liu, J.-H. Cho, Y. Jia and Z. Zhang, *Phys. Rev. Lett.*, 2017, **119**, 106101.
24 J. Chen, Y. Dai, Y. Ma, X. Dai, W. Ho and M. Xie, *Nanoscale*, 2017, **9**, 15945–15948.
25 E. J. Reed, *Nature*, 2017, **552**, 1–2.
26 Z. Xie, C. Xing, W. Huang, T. Fan, Z. Li, J. Zhao, Y. Xiang, Z. Guo, J. Li, Z. Yang, B. Dong, J. Qu, D. Fan and H. Zhang, *Adv. Funct. Mater.*, 2018, 1705833.
27 Y. Liu, W. Wu and W. A. Goddard, *J. Am. Chem. Soc.*, 2018, **140**, 550–553.
28 J. Qiao, Y. Pan, F. Yang, C. Wang, Y. Chai and W. Ji, *Sci. Bull.*, 2018, **63**, 159–168.
29 Y. Wang, G. Qiu, R. Wang, S. Huang, Q. Wang, Y. Liu, Y. Du, W. A. Goddard III, M. J. Kim, X. Xu, P. D. Ye and W. Wu, *Nat. Electron.*, 2018, **1**, 228–236.
30 M. S. Dresselhaus, G. Chen, M. Y. Tang, R. Yang, H. Lee, D. Wang, Z. Ren, J.-P. Fleurial and P. Gogna, *Adv. Mater.*, 2007, **19**, 1043–1053.
31 J. H. Seol, I. Jo, A. L. Moore, L. Lindsay, Z. H. Aitken, M. T. Pettes, X. Li, Z. Yao, R. Huang, D. Broido, N. Mingo, R. S. Ruoff and L. Shi, *Science*, 2010, **328**, 213–216.
32 A. A. Balandin, *Nat. Mater.*, 2011, **10**, 569–581.
33 A. D. Franklin, *Science*, 2015, **349**, aab2750.
34 H. Peng, N. Kioussis and D. A. Stewart, *Appl. Phys. Lett.*, 2015, **107**, 251904.
35 D. G. Cahill, S. K. Watson and R. O. Pohl, *Phys. Rev. B: Condens. Matter Mater. Phys.*, 1992, **46**, 6131.
36 Z. Gao, X. Dong, N. Li and J. Ren, *Nano Lett.*, 2017, **17**, 772–777.
37 X. Wu, V. Varshney, J. Lee, Y. Pang, A. K. Roy and T. Luo, *Chem. Phys. Lett.*, 2017, **669**, 233–237.
38 H. Peng, N. Kioussis and G. J. Snyder, *Phys. Rev. B: Condens. Matter Mater. Phys.*, 2014, **89**, 195206.
39 H. Goldsmid, *Thermoelectric refrigeration*, Plenum Press, 1964.
40 J. Carrete, W. Li, L. Lindsay, D. A. Broido, L. J. Gallego and N. Mingo, *Mater. Res. Lett.*, 2016, **4**, 204–211.
41 D. Liu, A. G. Every and D. Tománek, *Phys. Rev. B: Condens. Matter Mater. Phys.*, 2016, **94**, 165432.
42 L. Lindsay, D. A. Broido and N. Mingo, *Phys. Rev. B: Condens. Matter Mater. Phys.*, 2010, **82**, 115427.
43 Y. Xiao, C. Chang, Y. Pei, D. Wu, K. Peng, X. Zhou, S. Gong, J. He, Y. Zhang, Z. Zeng and L.-D. Zhao, *Phys. Rev. B: Condens. Matter Mater. Phys.*, 2016, **94**, 125203.
44 L. Lindsay and D. Broido, *J. Phys.: Condens. Matter*, 2008, **20**, 165209.
45 W. Li, J. Carrete, N. A. Katcho and N. Mingo, *Comput. Phys. Commun.*, 2014, **185**, 1747.
46 X. Gu and R. Yang, *Appl. Phys. Lett.*, 2014, **105**, 131903.
47 G. Qin, X. Zhang, S.-Y. Yue, Z. Qin, H. Wang, Y. Han and M. Hu, *Phys. Rev. B: Condens. Matter Mater. Phys.*, 2016, **94**, 165445.
48 Z. Gao, N. Li and B. Li, *Phys. Rev. E: Stat. Phys., Plasmas, Fluids, Relat. Interdiscip. Top.*, 2016, **93**, 022102.
49 Z. Gao, N. Li and B. Li, *Phys. Rev. E: Stat. Phys., Plasmas, Fluids, Relat. Interdiscip. Top.*, 2016, **93**, 032130.
50 M. Maldovan, *Nature*, 2013, **503**, 209.
51 C. Kittel, *Introduction to solid state physics*, Wiley, New York, 8th edn, 2004.
52 P. Klemens, *Solid state physics*, Elsevier, 1958, vol. 7, pp. 1–98.
53 J. S. Dugdale and D. K. C. MacDonald, *Phys. Rev.*, 1955, **98**, 1751–1752.
54 J. Callaway, *Phys. Rev.*, 1959, **113**, 1046–1051.
55 H. J. Goldsmid, *The thermal properties of solids*, Dover Publications, Inc., New York, 1965.
56 G. Kresse and J. Furthmüller, *Phys. Rev. B: Condens. Matter Mater. Phys.*, 1996, **54**, 11169–11186.
57 G. Kresse and J. Furthmüller, *Comput. Mater. Sci.*, 1996, **6**, 15.
58 J. P. Perdew, K. Burke and M. Ernzerhof, *Phys. Rev. Lett.*, 1996, **77**, 3865–3868.
59 P. E. Blöchl, *Phys. Rev. B: Condens. Matter Mater. Phys.*, 1994, **50**, 17953–17979.
60 G. Kresse and D. Joubert, *Phys. Rev. B: Condens. Matter Mater. Phys.*, 1999, **59**, 1758–1775.
61 L. Lindsay, D. A. Broido and T. L. Reinecke, *Phys. Rev. Lett.*, 2012, **109**, 095901.
62 A. Togo, F. Oba and I. Tanaka, *Phys. Rev. B: Condens. Matter Mater. Phys.*, 2008, **78**, 134106.
63 W. Li, N. Mingo, L. Lindsay, D. A. Broido, D. A. Stewart and N. A. Katcho, *Phys. Rev. B: Condens. Matter Mater. Phys.*, 2012, **85**, 195436.
64 W. Li, L. Lindsay, D. A. Broido, D. A. Stewart and N. Mingo, *Phys. Rev. B: Condens. Matter Mater. Phys.*, 2012, **86**, 174307.